

Gravitational waves triggered by $B - L$ charged hidden scalar and leptogenesis

Ligong Bian,^a Wei Cheng,^b Huai-Ke Guo,^c Yongchao Zhang^{d,e}

^a*Department of Physics, Chongqing University, Chongqing 401331, China*

^b*State Key Laboratory of Theoretical Physics, Institute of Theoretical Physics, Chinese Academy of Sciences, Beijing, 100190, China*

^c*Department of Physics and Astronomy, University of Oklahoma, Norman, OK 73019, USA*

^d*Department of Physics and McDonnell Center for the Space Sciences, Washington University, St. Louis, MO 63130, USA*

^e*Center for High Energy Physics, Peking University, Beijing 100871, China*

E-mail: lgbycl@cqu.edu.cn, chengwei@itp.ac.cn, ghk@ou.edu,
yongchao.zhang@physics.wustl.edu

ABSTRACT: We study the electroweak symmetry breaking in the framework of a classically conformal $U(1)_{B-L}$ theory, where three right-handed neutrinos (RHNs) and a hidden scalar are introduced, with the latter playing the role of dark matter (DM). It is found that the DM and RHN sectors are crucial for the spontaneous symmetry breaking of the $U(1)_{B-L}$ symmetry, strong first order phase transition in the conformal theory and the resultant gravitational wave (GW) prospects at future space-based interferometer LISA and other GW experiments. The baryon asymmetry of the Universe is addressed by the resonant leptogenesis mechanism, which is potentially disturbed by the hidden scalar. To make the GW spectra detectable by LISA and resonant leptogenesis work in the conformal $U(1)_{B-L}$ theory, the hidden scalar can not fully saturate the observed DM relic density.

Contents

1	Introduction	1
2	The conformal $U(1)_{B-L}$ model	3
2.1	The basic setup	3
2.2	Limits from vacuum stability and perturbativity	5
2.3	Current Z' limits	6
3	Phase transition dynamics and gravitational wave signatures	8
3.1	Dynamical $U(1)_{B-L}$ breaking and phase transition	8
3.2	Gravitational waves signals	9
4	Resonant Leptogenesis	12
5	WIMP DM in the conformal $U(1)_{B-L}$ model	16
5.1	Relic density and direct detection	16
5.2	Collider signatures	17
6	Conclusion	17
A	Renormalization group equations	18
B	Reduced cross sections for leptogenesis	19
C	DM annihilation cross section	20

1 Introduction

Since the discovery of the standard model (SM) Higgs at the Large Hadron Collider (LHC), understanding the hierarchy problem becomes one of the most challenging theoretical difficulties in the SM, i.e. why the SM Higgs mass is much lower than the Planck scale? In light of null result in searches of new heavy particles at LHC, in particular the supersymmetric particles, the hierarchy problem is getting more concerned. This is also intimately related to the spontaneous electroweak symmetry breaking (EWSB), which is responsible for the generation of SM particle masses, and underlying more fundamental theories. One elegant way out is the Coleman-Weinberg mechanism [1], in which the original potential is classically conformal and the EWSB is induced when the mass term is generated radiatively. As the conformal scale invariant version of the SM is not consistent with the Higgs data,

one may take advantage of the Higgs-portal and therefore obtain a natural EWSB [2, 3]. The possibility to accommodate dark matter (DM) particles and inflation has been considered [4], where extra scalar fields are introduced which are charged under the conformal $U(1)_{B-L}$ gauge group extension of the SM and are viable DM candidates [5].

The $U(1)_{B-L}$ symmetry breaking process could be dynamical while the Universe cools down, i.e. being a phase transition process. When the phase transition is first order, gravitational waves (GWs) could be generated and detected in current and future GW experiments, such as LISA [6, 7], Taiji [8], TianQin [9], Big Bang Observer (BBO) [10], DECi-hertz Interferometer Gravitational wave Observatory (DECIGO) [11] and Ultimate-DECIGO [12]. For the study of the GW signal predictions within this framework, see e.g., Ref. [13–18]. Where the $B - L$ symmetry can break at the TeV scale or under QCD scale after the QCD phase transition.

For the purpose of gauge anomaly cancellation, three right-handed neutrinos (RHNs) N_i (with $i = 1, 2, 3$) are introduced to the $U(1)_{B-L}$ model, which can be used to generate the tiny neutrino masses via the type-I seesaw mechanism [19–23]. Furthermore, the lepton asymmetry can be generated from the CP violating decays of heavy RHNs, i.e. through the mechanism of leptogenesis [24], which is then transferred into the baryon asymmetry through electroweak sphaleron processes. For the studies of leptogenesis in conformal theories, see e.g. Ref. [25]. If only one RHN is involved in leptogenesis, the RHN is too heavy to be produced at colliders, and we consider the TeV-scale resonant leptogenesis with two mass quasi-degenerate RHNs [26–29]. As the RHNs couples to the scalar Φ and the heavy Z' gauge boson which is from the $U(1)_{B-L}$ symmetry breaking, the processes $NN \rightarrow f\bar{f}, \Phi\Phi, \Phi Z'$ (with f the SM fermions) will dilute the heavy RHNs by two units, thus reducing the lepton and baryon asymmetry significantly [30–35].

When a scalar \mathcal{S} with nontrivial $B - L$ charge is introduced to the $U(1)_{B-L}$ model, it could be a viable DM candidate if it does not develop a non-vanishing vacuum expectation value (VEV). See Ref. [36] for a supercool DM scenario where the GW signal from phase transition is quite different from our scenario. In this work, the scalar \mathcal{S} has nontrivial $B - L$ charges and its $B - L$ charge should be $n_x \neq \pm 2n$ with n being an integer and smaller than 4 such that the neutral DM scalar can be stabilized by the accidental $B - L$ symmetry [37]. As a result of the $B - L$ charge of \mathcal{S} , the leptogenesis diffusion process can be disturbed and the annihilation process $NN \rightarrow \mathcal{S}\mathcal{S}^\dagger$ is also important. This dilution effect falsifies leptogenesis in a large region of parameter space (see Fig. 5). Even though the DM scalar \mathcal{S} and its complex conjugate \mathcal{S}^\dagger can be pair produced through both the scalar and gauge portals, the monojet and other DM searches at the LHC are too weak to exclude any parameter space [38–41]. However, we find that the DM scalar \mathcal{S} and the RHNs and their couplings play an important role in the phase transition and GW emission. We estimate the possibility of whether the DM (hidden) scalar can saturate the DM relic abundance and at the same time satisfy the current limits from low-background direct DM

Table 1. Particle content of the conformal $U(1)_{B-L}$ model: In addition to the SM particles, there are three RHNs N_i ($i = 1, 2, 3$), a complex singlet scalar Φ and another complex singlet scalar \mathcal{S} .

	$SU(3)_c$	$SU(2)_L$	$U(1)_Y$	$U(1)_{B-L}$
q_L^i	3	2	+1/6	+1/3
u_R^i	3	1	+2/3	+1/3
d_R^i	3	1	-1/3	+1/3
ℓ_L^i	1	2	-1/2	-1
N_i	1	1	0	-1
e_R^i	1	1	-1	-1
H	1	2	+1/2	0
Φ	1	1	0	+2
\mathcal{S}	1	1	0	n_x

searches, i.e. those from LUX [42], PandaX-II [43, 44] and Xenon1T [45].

This work is organized as follows: In Section 2 we introduce the $B - L$ extension of the SM with classical conformal symmetry, where the hidden scalar could be stabilized depending on its $B - L$ charge. In this section we consider also the limits from vacuum stability and perturbativity as well as the current collider constraints on Z' boson. The cosmological symmetry breaking history and the GWs generated during the phase transition are investigated in Section 3. The impact of the hidden scalar on resonant leptogenesis is studied in the Section 4. The relic abundance of the hidden scalar in the $U(1)_{B-L}$ model is explored in Section 5, where we also comment briefly on the collider search of the DM particle, before we conclude in Section 6. The renormalization group equations (RGEs), the (reduced) cross sections for leptogenesis and DM annihilation are collected in the appendices.

2 The conformal $U(1)_{B-L}$ model

2.1 The basic setup

The particle content of the conformal $U(1)_{B-L}$ model is presented in Table 1, where the q_L , u_R and d_R are the SM quark doublets and singlets, ℓ_L and e_R the SM lepton doublets and singlets, and H is the SM-like Higgs doublet. Three RHNs N_i , a complex singlet scalar Φ with $B - L$ charge of 2 and a complex singlet scalar \mathcal{S} with $B - L$ charge of n_x are introduced to the model. To implement the EWSB, the most general scalar potential for the fields H and Φ reads, which is classically scale invariant,

$$V_{\text{cl}}(H, \phi) = \lambda_H(H^\dagger H)^2 + \lambda_\phi(\Phi^\dagger \Phi)^2 - \lambda_P(H^\dagger H)(\Phi^\dagger \Phi). \quad (2.1)$$

When the scalar \mathcal{S} couples to the fields H and Φ via the scalar portal interactions, the full scalar potential is

$$V_{\text{cl}}(H, \phi, \mathcal{S}) = V_{\text{cl}}(H, \Phi) + \lambda_{HS}(H^\dagger H)(\mathcal{S}^\dagger \mathcal{S}) + \lambda_{\phi\mathcal{S}}(\Phi^\dagger \Phi)(\mathcal{S}^\dagger \mathcal{S}) + \lambda_{\mathcal{S}}(\mathcal{S}^\dagger \mathcal{S})^2. \quad (2.2)$$

After spontaneous symmetry breaking, the Φ and H fields develop non-vanishing VEVs, which are respectively

$$\langle \Phi \rangle = \frac{1}{\sqrt{2}} v_{BL}, \quad \langle H^0 \rangle = \frac{1}{\sqrt{2}} v_{\text{EW}}, \quad (2.3)$$

with H^0 the neutral component of the doublet H . For simplicity, all the coupling coefficients in the potential (2.2) are assumed to be positive. In addition, the positivity of λ_{HS} and $\lambda_{\phi\mathcal{S}}$ ensures that no VEV is generated for the hidden scalar \mathcal{S} , which is a necessary condition for \mathcal{S} to be a DM candidate. In the unitarity gauge, we have the following physical scalars $H = (0, h/\sqrt{2})$, $\Phi = \phi/\sqrt{2}$, \mathcal{S} and its complex conjugate \mathcal{S}^\dagger . With the $B - L$ charge of 2, the Φ scalar can give masses to the RHNs, through the Y_ϕ Yukawa interactions below

$$\mathcal{L}_{\text{Yukawa}} \supset Y_D \bar{\ell} H N + \frac{1}{2} Y_\phi \overline{N^C} \Phi N + \text{H.c.}, \quad (2.4)$$

where we do not show explicitly the flavor indices for the sake of clarity, and C is the charge conjugate operator. In Eq. (2.4), the Y_D term is responsible for the Dirac neutrino mass matrix, and the tiny neutrino masses are generated through the type-I seesaw mechanism $m_\nu = -Y_D m_N^{-1} Y_D^\top v_{\text{EW}}^2/2$, with $M_N = Y_\phi v_{BL}/\sqrt{2}$ the RHN mass matrix.

When the 1-loop corrections are taken into consideration, the effective potential for the ϕ field is

$$V_1(\phi; \mu) = \frac{\lambda_\phi(\mu)}{4} \phi^4 + \frac{\beta_{\lambda_\phi}}{8} \phi^4 \left(\log \frac{\phi^2}{\mu^2} - \frac{25}{6} \right) - \frac{\lambda_P(\mu)}{4} h^2 \phi^2, \quad (2.5)$$

where the couplings λ_ϕ and λ_P depend on the energy scale μ , and the exact expression for the coefficient β_{λ_ϕ} is given in Eq. (A.3). Minimizing the potential in Eq. (2.5) at the scale $\mu = v_{BL}$ gives the matching condition for the couplings; and expanding the terms in Eq. (2.5) around the vacuum at v_{BL} determines the mass of the Coleman-Weinberg field ϕ , giving rise to

$$\lambda_\phi(v_{BL}) = \frac{11}{6} \beta_{\lambda_\phi}, \quad (2.6)$$

and the potential can be simplified to be

$$V_1(\phi; v_{BL}) = \beta_{\lambda_\phi} \phi^4 \left[2 \log \left(\frac{\phi^2}{v_{BL}^2} \right) - 1 \right]. \quad (2.7)$$

After symmetry breaking at the $U(1)_{BL}$ scale we obtain the following mass for the $U(1)_{B-L}$ gauge boson Z'

$$M_{Z'} = 2g_{BL} v_{BL}, \quad (2.8)$$

where g_{BL} is the gauge coupling for the $U(1)_{B-L}$ gauge group. The ϕ field mass is therefore given by

$$m_\phi^2 = \beta_{\lambda_\phi} v_{BL}^2 \approx \frac{4m_S^4 - m_N^4 + 6M_{Z'}^4}{16\pi^2 v_{BL}^2}, \quad (2.9)$$

where we have applied the relation $\beta_{\lambda_\phi} \approx (96g_{BL}^4 + \lambda_{\phi S}^2 - Y_\phi^4)/16\pi^2$, and m_N and m_S are respectively the masses for RHNs and the \mathcal{S} scalar. One can see from Eq. (2.9) that correct spontaneous symmetry breaking of the $U(1)_{B-L}$ symmetry requires that $4m_S^4 + 6m_{Z'}^4 > m_N^4$. Supposing Y_ϕ is much smaller than g_{BL} and $\lambda_{\phi S}$ which implies that the RHNs are much lighter than the v_{BL} scale, we have

$$m_\phi^2 \approx \frac{4m_S^4 + 6M_{Z'}^4}{16\pi^2 v_{BL}^2}. \quad (2.10)$$

If both the contributions of $\lambda_{\phi S}$ and Y_ϕ to β_{λ_ϕ} are negligible, then

$$m_\phi^2 \approx \frac{6M_{Z'}^4}{16\pi^2 v_{BL}^2}. \quad (2.11)$$

A non-vanishing VEV of the ϕ field will generate the following mass parameters for the scalar potential in Eq. (2.1), which is essential for the spontaneous EWSB,

$$\mu_H^2 = -\frac{1}{2}\lambda_P v_{BL}^2, \quad \mu_S^2 = +\frac{1}{2}\lambda_{\phi S} v_{BL}^2. \quad (2.12)$$

The VEV v_{BL} also generates the mass term for the \mathcal{S} field:

$$m_S^2 = \frac{1}{2}\lambda_{\phi S} v_{BL}^2, \quad (2.13)$$

in the vacuum $S = 0$, $\langle \phi \rangle = v_{BL}$, $\langle H^0 \rangle = v_{EW}/\sqrt{2} = \sqrt{\lambda_P/\lambda_H} v_{BL}$. This relation is justified when the quartic coupling λ_{HS} is sufficiently small, and therefore the EWSB contribution to m_S^2 , i.e. the $\lambda_{HS} v^2$ term, is negligible. Here we stress that the μ_S^2 term can also be negative and thus one can expect a local minimum in the direction of S . The expressions for the electroweak VEV v_{EW} and the Higgs mass m_h are analogous to the SM case.

2.2 Limits from vacuum stability and perturbativity

For the sake of completeness we check the limits on the conformal $U(1)_{B-L}$ model from vacuum stability and perturbativity. The one-loop RGEs for all the quartic, Yukawa and gauge couplings are collected in Appendix A, and the tree-level stability conditions are given as below, which is consistent with that given in Ref. [46]:

$$\begin{aligned} \lambda_H &\geq 0, \quad \lambda_\phi \geq 0, \quad \lambda_S \geq 0, \\ 2\sqrt{\lambda_H \lambda_\phi} - \lambda_P &\geq 0, \quad \lambda_{HS} - 2\sqrt{\lambda_H \lambda_S} \geq 0, \quad \lambda_{\phi S} - 2\sqrt{\lambda_\phi \lambda_S} \geq 0, \\ \sqrt{-\lambda_P + 2\sqrt{\lambda_H \lambda_\phi}} \sqrt{\lambda_{HS} + 2\sqrt{\lambda_H \lambda_S}} \sqrt{\lambda_{\phi S} + 2\sqrt{\lambda_\phi \lambda_S}} \\ + 2\sqrt{\lambda_H \lambda_\phi \lambda_S} - \lambda_P \sqrt{\lambda_S} + \lambda_{HS} \sqrt{\lambda_\phi} + \lambda_{\phi S} \sqrt{\lambda_H} &\geq 0. \end{aligned} \quad (2.14)$$

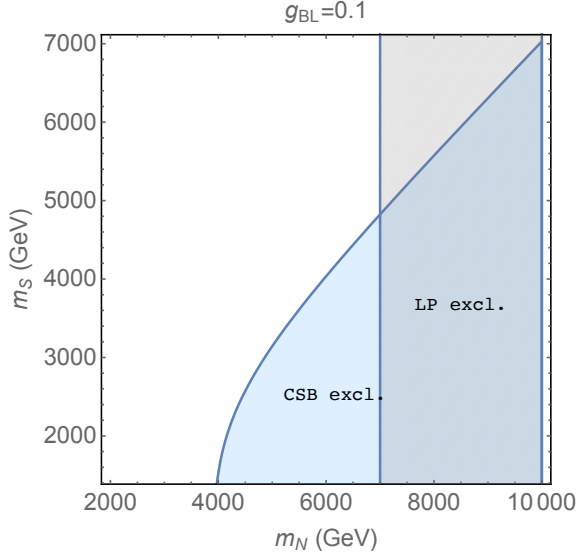


Figure 1. The Landau pole and vacuum stability excluded regions for the $g_{BL} = 0.1$ scenario given in Fig. 3.

From these equations and relations we can find the Landau pole and vacuum stability bounds on the quartic scalar couplings, the $U(1)_{B-L}$ gauge couplings g_{BL} , and the $B-L$ charge n_x of the hidden scalar \mathcal{S} . With the initial conditions for all SM couplings at the SM scale $\mu = m_t$ (with m_t the top quark mass), we run all the couplings up to the Planck scale $\mu = M_{\text{Pl}} = 1.22 \times 10^{19}$ GeV using the RGEs.

We study three different scenarios of the $U(1)_{B-L}$ which is shown in Fig. 3 and to be compared to the current LHC constraints on the Z' boson and future GW prospects. It turns out that the vacuum stability issue is not going to be much better than in the SM, since the GW prospects of the conformal $U(1)_{B-L}$ model prefer small quartic couplings of $\lambda_{HS,P}$, and a large Yukawa coupling Y_ϕ for the RHNs would result in a Landau pole problem, since they tend to dominate the running of the quartic couplings at sufficiently high scale. The Landau pole appears at a scale much lower than M_{Pl} for both the second and third benchmark scenarios in Fig. 3; as a comparison, the first scenario is much better, benefitting from a smaller coupling $g_{BL} = 0.1$. The vacuum stability and Landau pole limits on the RHN mass m_N and the DM mass m_S are shown in Fig. 1, where we have set $n_x = 1$.

2.3 Current Z' limits

For a TeV-scale v_{BL} , the Z' mass is stringently constrained by the dilepton data $pp \rightarrow Z' \rightarrow \ell^+\ell^-$ (with $\ell = e, \mu$) at the LHC [47, 48]. For a sequential Z' boson with the same couplings as in the SM, the current ATLAS and CMS 13 TeV data requires that $M_{Z'} > 4.05$ TeV at the 95% confidence level [49, 50]. The production cross section $\sigma(pp \rightarrow Z' \rightarrow \ell^+\ell^-)$ in the $U(1)_{B-L}$ model can be obtained by rescaling that of a sequential heavy Z' boson, as a function of the gauge coupling g_{BL} [51]. To this end, the partial decay widths of the Z'

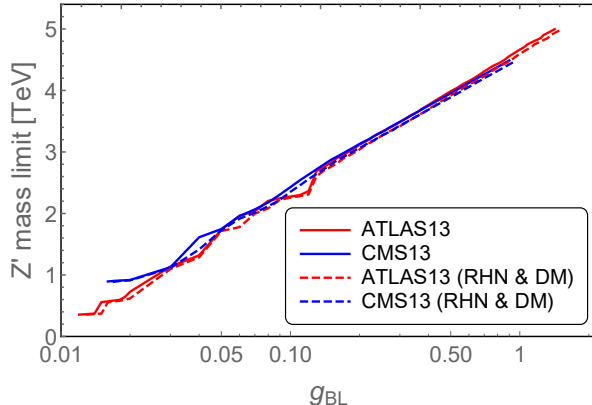


Figure 2. Dilepton limits on the Z' boson mass from the 13 TeV data by ATLAS [49] (red) and CMS [50] (blue), as function of the gauge coupling g_{BL} . The solid curves assume that the Z' boson decays only into the SM fermions, while for the dashed curves Z' decays also into the three RHNs and DM.

boson into the SM fermions, the heavy RHNs and the scalar \mathcal{S} are respectively

$$\begin{aligned}
 \Gamma(Z' \rightarrow f\bar{f}) &= \frac{S_f N_C^f (B_f - L_f)^2 g_{BL}^2 M_{Z'}}{48\pi}, \\
 \Gamma(Z' \rightarrow NN) &= \frac{g_{BL}^2 M_{Z'}}{96\pi} \left(1 - \frac{4m_N^2}{M_{Z'}^2}\right)^{3/2}, \\
 \Gamma(Z' \rightarrow \mathcal{S}\mathcal{S}^\dagger) &= \frac{n_x^2 g_{BL}^2 M_{Z'}}{192\pi} \left(1 - \frac{4m_{\mathcal{S}}^2}{M_{Z'}^2}\right)^{3/2},
 \end{aligned} \tag{2.15}$$

with N_C the color factor (3 for quarks and 1 otherwise), B_f and L_f the baryon and lepton numbers for the SM fermions, $S_f = 1$ for the quarks and charged leptons and 1/2 for the light neutrinos. All these decay modes are universally proportional to the gauge coupling g_{BL} . In the absence of the heavy RHNs and the \mathcal{S} field, the branching fraction $\text{BR}(Z' \rightarrow \ell^+\ell^-)$ is a constant, being 8/23, in the limit of $M_{Z'} \gg m_f$, and the production cross section $\sigma(pp \rightarrow Z') \propto g_{BL}^2$. As a result, when g_{BL} gets larger, the dilepton limits on the Z' mass tend to be stronger. The constraints from the ATLAS [49] and CMS [50] 13 TeV data are shown respectively as the solid red and blue curves in Fig. 2. As a comparison, we also show in Fig. 2 the dilepton limits in the presence of the three RHNs and DM as the dashed curves, assuming their masses are significantly lower than $M_{Z'}/2$ thus the decays $Z' \rightarrow NN, \mathcal{S}\mathcal{S}^\dagger$ are kinematically allowed. As a result of these extra decays modes, the dilepton limits in Fig. 2 become slightly weaker. For illustration purpose, we adopt three different benchmark values of $g_{BL} = 0.1, 0.3$ and 1.0 , interpret the solid lines in Fig. 2 and obtain the current dilepton constraints on the Z' boson mass and the corresponding limits on v_{BL} , which are collected in Table 2. At the high-luminosity LHC (HL-LHC) and future 100 TeV colliders, the prospects of the Z' boson could be largely improved [52–54].

Table 2. The lower bounds on the Z' boson mass $M_{Z'}$ and the v_{BL} scale in the $U(1)_{B-L}$ model from the current LHC13 data [49, 50] (cf. Fig. 2).

g_{BL}	without RHNs & DM		with RHNs & DM	
	$M_{Z'}$ [TeV]	v_{BL} [TeV]	$M_{Z'}$ [TeV]	v_{BL} [TeV]
0.1	2.42	17.2	2.35	16.6
0.3	3.49	8.22	3.43	8.08
1.0	4.66	3.30	4.59	3.25

3 Phase transition dynamics and gravitational wave signatures

As the Universe cools down, the EWSB is induced by the dynamical breaking of the $U(1)_{B-L}$, i.e., phase transition. If the phase transition is strong first order, GWs can be produced and potentially probed by the space-based interferometers like LISA.

3.1 Dynamical $U(1)_{B-L}$ breaking and phase transition

In this section, we first demonstrate the calculation of the phase transition, which is determined by the thermal potential. The finite temperature corrections to the effective potential at one loop are given by

$$V_1(\phi, T) = \frac{T^4}{2\pi^2} \sum_i n_i J_{B,F} \left(\frac{M_i^2(\phi)}{T^2} \right) \quad (3.1)$$

where the functions $J_{B,F}(y)$ are

$$J_{B,F}(y) = \pm \int_0^\infty dx x^2 \ln \left[1 \mp \exp \left(-\sqrt{x^2 + y} \right) \right] \quad (3.2)$$

with the upper (lower) sign corresponding to bosonic (fermionic) contributions. Here, in order to describe the high- T and low- T behaviors appropriately, the above integrals $J_{B,F}$ can be expressed as a sum of the second kind of modified Bessel functions $K_2(x)$ [55],

$$J_{B,F}(y) = \lim_{N \rightarrow +\infty} \mp \sum_{l=1}^N \frac{(\pm 1)^l y}{l^2} K_2(\sqrt{yl}) . \quad (3.3)$$

The dominant contributions come from the hidden scalar \mathcal{S} , RHNs N_i and the extra gauge field Z' . The field dependent mass and thermal corrections are given respectively by

$$m_S^2 = \frac{\lambda_{\phi S}}{2} \phi^2, \quad m_{Z'}^2 = 4g_{B-L}^2 \phi^2, \quad (3.4)$$

$$\Pi_{Z'} = 4g_{B-L}^2 T^2, \quad \Pi_S = (g_{B-L}^2 + \frac{\lambda_{\phi S}}{12}) T^2, \quad \Pi_\phi = (\frac{\lambda_{\phi S}}{12} + g_{B-L}^2 + Y_\phi^2) T^2. \quad (3.5)$$

3.2 Gravitational waves signals

The bounce configuration of the nucleated bubble, i.e. the bounce configuration of the field that connects the $U(1)_{B-L}$ broken vacuum (true vacuum) and the false vacuum (here it can be $U(1)_{B-L}$ conserving vacuum), can be obtained by extremizing

$$S_3(T) = \int 4\pi r^2 dr \left[\frac{1}{2} \left(\frac{d\phi_b}{dr} \right)^2 + V(\phi_b, T) \right] \quad (3.6)$$

through solving the equation of motion for ϕ_b (it is ϕ for the scenario under study),

$$\frac{d^2\phi_b}{dr^2} + \frac{2}{r} \frac{d\phi_b}{dr} - \frac{\partial V(\phi_b)}{\partial \phi_b} = 0, \quad (3.7)$$

with the boundary conditions of

$$\lim_{r \rightarrow \infty} \phi_b = 0, \quad \left. \frac{d\phi_b}{dr} \right|_{r=0} = 0. \quad (3.8)$$

At the nucleation temperature T_n , the thermal tunneling probability for bubble nucleation per horizon volume and per horizon time is of order unity with [56–58],

$$\Gamma \approx A(T) e^{-S_3/T} \sim 1. \quad (3.9)$$

Two parameters are crucial for the calculations of GW emission:

- The parameter α . It describes the strength of the phase transition, and is defined as the energy density released from the strong first order EWPT normalized by the total radiation energy density $\rho_R = \pi^2 g_* T_*^4/30$:

$$\alpha = \frac{\Delta\rho}{\rho_R}, \quad (3.10)$$

where $\Delta\rho$ is the latent heat released in phase transition, i.e. the difference of the energy density between the false and the true vacuum.

- The parameter β . It describes roughly the inverse time duration of the strong first order EWPT, and characterizes the GW spectrum peak frequency, which is connected with the action S_3 through

$$\frac{\beta}{H_n} = T \left. \frac{d(S_3(T)/T)}{dT} \right|_{T=T_n}, \quad (3.11)$$

where H_n is the Hubble parameter at the bubble nucleation temperature T_n .

We are now ready to calculate the stochastic GW background generated during the first order phase transition. Significant progress has been made in recent years on the calculations of the GW from phase transitions (see e.g. Ref. [59–61] for recent reviews). It is now generally believed that the dominant source for the GW production in this process is the

sound waves (SWs) in the plasma which lasts long after the phase transition completes [62, 63], though the bubble collision contribution has also been theoretically well modeled [64–71]. Another contribution comes from the Magnetohydrodynamic (MHD) turbulence in the magnetized plasma with high Reynolds number [72, 73]. The total resultant energy density spectrum can be approximated by the following linear summation of the individual contributions above:

$$\Omega_{\text{GW}}h^2 \simeq \Omega_{\text{col}}h^2 + \Omega_{\text{sw}}h^2 + \Omega_{\text{turb}}h^2, \quad (3.12)$$

and we neglect in the following the contribution from bubble collision Ω_{col} .

The GW spectrum from the dominant SWs can be found by fitting to the result of numerical simulations with the fluid-scalar field model [63]:

$$\begin{aligned} \Omega_{\text{sw}}h^2 &= 2.65 \times 10^{-6} \left(\frac{H_n}{\beta}\right)^2 \left(\frac{\kappa_v \alpha}{1 + \alpha}\right)^2 \left(\frac{100}{g_*}\right)^{1/3} \\ &\times v_w \left(\frac{f}{f_{\text{sw}}}\right)^3 \left(\frac{7}{4 + 3(f/f_{\text{sw}})^2}\right)^{7/2}, \end{aligned} \quad (3.13)$$

where g_* is the relativistic degrees of freedom in the plasma at the time of EWPT and f_{sw} is the present peak frequency of the spectrum:

$$f_{\text{sw}} = 1.9 \times 10^{-5} \frac{1}{v_w} \left(\frac{\beta}{H_n}\right) \left(\frac{T_n}{100\text{GeV}}\right) \left(\frac{g_*}{100}\right)^{1/6} \text{Hz}. \quad (3.14)$$

In addition, the factor κ_v is the fraction of latent heat transformed into the kinetic energy of the fluid and can be found by solving the hydrodynamic velocity profiles of the bubbles [74–76].

The GW spectrum from the MHD turbulence can be theoretically modelled with inputs of the magnetic and turbulence power spectra [72, 77–79] and improved by numerically evolving the MHD equations [80, 81]. A fitting formula is also available [72, 73]:

$$\begin{aligned} \Omega_{\text{turb}}h^2 &= 3.35 \times 10^{-4} \left(\frac{H_n}{\beta}\right)^2 \left(\frac{\kappa_{\text{turb}} \alpha}{1 + \alpha}\right)^{3/2} \left(\frac{100}{g_*}\right)^{1/3} \\ &\times v_w \frac{(f/f_{\text{turb}})^3}{[1 + (f/f_{\text{turb}})]^{11/3} (1 + 8\pi f/h_*)}. \end{aligned} \quad (3.15)$$

Here the peak frequency f_{turb} is given by

$$f_{\text{turb}} = 2.7 \times 10^{-5} \frac{1}{v_w} \left(\frac{\beta}{H_n}\right) \left(\frac{T_n}{100\text{GeV}}\right) \left(\frac{g_*}{100}\right)^{1/6} \text{Hz}. \quad (3.16)$$

The energy fraction transferred to the MHD turbulence κ_{turb} is uncertain as of now and can vary between 5% to 10% of κ_v [63]. Here we take tentatively $\kappa_{\text{turb}} = 0.1\kappa_v$.

Summing up the results in Eqs. (3.13) and (3.15), we can obtain the total GW energy density spectrum. The expected GW energy spectra for three benchmark scenarios with different g_{BL} values are shown in Fig. 3. The color-shaded regions on the top are the experimentally sensitive regions for several proposed space-based GW detectors. As discussed

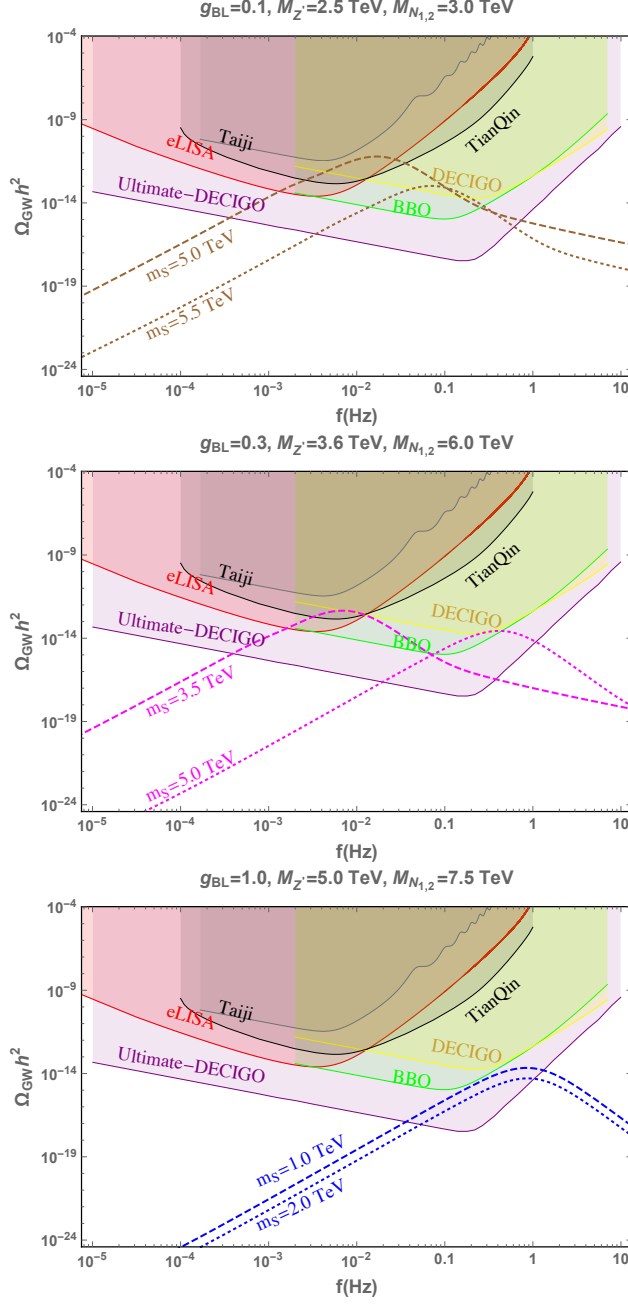


Figure 3. The expected GW spectra for three benchmark scenarios in the conformal $U(1)_{B-L}$ model, shown as the dashed curves, with respectively $g_{BL} = 0.1$ (top), 0.3 (middle) and 1 (bottom). The shaded regions demonstrate the prospects for different GW experiments.

earlier, the GW signal comes mainly from SWs. Our study indicates that increasing the RHN masses may leads to a decrease of the phase transition temperature, while its mass is severely bounded by the EWSB conditions given in Eq. (2.9). The three panels of Fig. 3 demonstrate that the amplitudes of GW signal spectra decrease as g_{BL} increases, which

implies that the GW prospects are weaker when the $B - L$ charge of DM scalar is large. The hidden scalar \mathcal{S} is useful for generating the proper vacuum barrier at the nucleation temperature. Furthermore, a larger hidden scalar mass leads to a lower GW amplitude and a higher peak frequency for the GW spectrum.

To assess the discovery prospects of the GW spectra, we calculate the signal-to-noise ratio (SNR) with the definition adopted by Ref. [59]:

$$\text{SNR} = \sqrt{\mathcal{T} \int_{f_{\min}}^{f_{\max}} df \left[\frac{h^2 \Omega_{\text{GW}}(f)}{h^2 \Omega_{\text{exp}}(f)} \right]^2}, \quad (3.17)$$

where $h^2 \Omega_{\text{exp}}(f)$ is the experimental sensitivity for the detectors and \mathcal{T} is the mission duration in unit of year for each experiment. Here we assume $\mathcal{T} = 5$. For the LISA configurations with four links, the suggested threshold SNR for discovery is 50 [59]. For the six link configurations as drawn here, the uncorrelated noise reduction technique can be used and the suggested SNR threshold can be as low as 10 [59]. The GW spectrum of the $m_S = 5.0$ TeV case for the $g_{BL} = 0.1$ and $g_{BL} = 0.3$ scenarios are able to be detected by LISA, with respectively $\text{SNR} = 22$ and $\text{SNR} = 5$.

4 Resonant Leptogenesis

For the case of leptogenesis occurring via flavor oscillations of the heavy right-handed neutrinos in the classically conformal models, we refer the readers to Ref. [25] to look for some details. For TeV scale RHNs, it is necessary to use the resonant leptogenesis mechanism [26–29] in order to avoid the Davidson-Ibarra bound [82]. For simplicity, we assume the two RHN mass eigenstates N_1 and N_2 are almost degenerate with the mass m_N and a small splitting $\Delta m_N/m_N \ll 1$, and the third RHN N_3 significantly heavier. The heavy Z' boson, the conformal scalar ϕ and the DM scalar \mathcal{S} play important roles in the generation of lepton asymmetry from the decay of RHNs, as they would induce processes that dilute the heavy RHNs by two units, thus reducing the lepton and baryon asymmetry significantly in a large regions of parameter space [30–35]. Such $\Delta N = 2$ processes include

$$NN \rightarrow f\bar{f}, Z'\phi, \phi\phi, \mathcal{S}\mathcal{S}^\dagger, \quad (4.1)$$

with f running over all the flavors of SM quarks, charged leptons and neutrinos. The corresponding Feynman diagrams are shown in Fig. 4. One should note that the scalar mixing between h and ϕ however does not play any role in freeze-out leptogenesis since the latter takes place prior to EWSB. Thus the processes $NN \rightarrow f\bar{f}$ are only mediated by the Z' gauge boson. The Feynman diagrams $NN \rightarrow Z'\phi$ in (b) and (c) are mediated by the gauge and Yukawa couplings, the process $NN \rightarrow \phi\phi$ in (d) and (e) by the Yukawa couplings and the scalar quartic coupling λ_ϕ in the potential (1.4). If the DM \mathcal{S} is lighter than the RHNs $N_{1,2}$, i.e. $m_S \lesssim m_N$, the process $NN \rightarrow \mathcal{S}\mathcal{S}^\dagger$ in (f) and (g) is also important in some

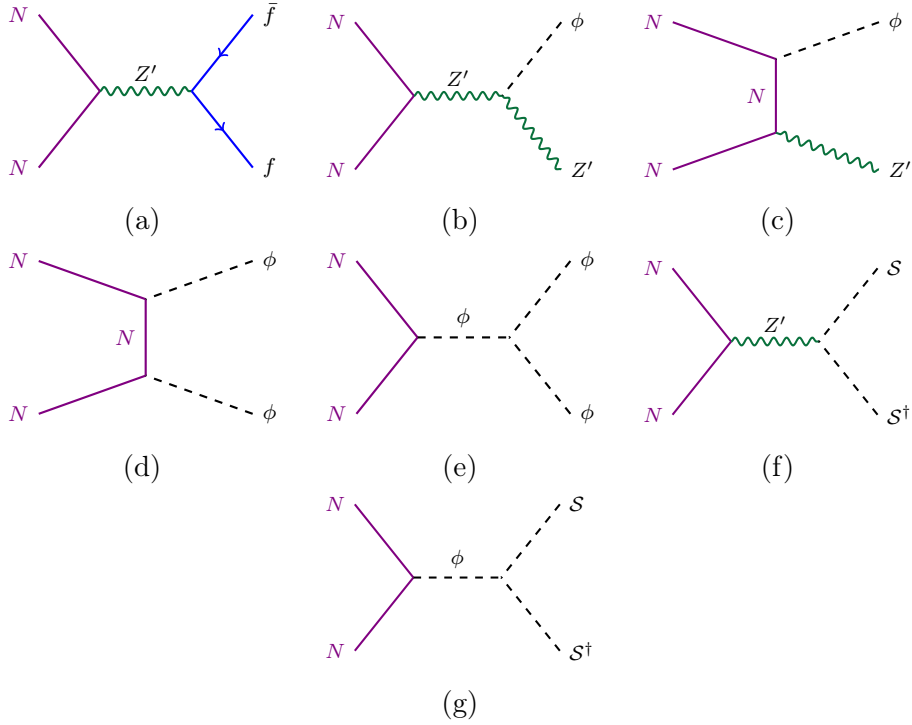


Figure 4. Feynman diagram for the process (a) $NN \rightarrow f\bar{f}$, (b) and (c) $NN \rightarrow Z'\Phi$, (d) and (e) $NN \rightarrow \Phi\Phi$, and (f) and (g) $NN \rightarrow \mathcal{S}\mathcal{S}^\dagger$.

region of the parameter space, which is induced through both the gauge (Z') and scalar (ϕ) portals. There exists in principle also the process $NN \rightarrow Z'Z'$. However, in the conformal theories the RHN masses are constrained as shown in Eq. (2.9); with N_3 heavier than $N_{1,2}$ and neglecting the DM mass, Eq. (2.9) implies that $m_N = m_{N_{1,2}} < 2^{1/8}M_{Z'} \simeq 1.09M_{Z'}$. Then the process $NN \rightarrow Z'Z'$ process is insignificant, suppressed by the kinematical space.

The Boltzmann equations, which govern the evolution of the RHN number density and the lepton asymmetry, are given by

$$\frac{n_\gamma H_N}{z} \frac{d\eta_N}{dz} = - \left[\left(\frac{\eta_N}{\eta_N^{\text{eq}}} \right)^2 - 1 \right] 2\gamma_{NN} - \left(\frac{\eta_N}{\eta_N^{\text{eq}}} - 1 \right) [\gamma_D + \gamma_s + 2\gamma_t], \quad (4.2)$$

$$\frac{n_\gamma H_N}{z} \frac{d\eta_{\Delta L}}{dz} = \gamma_D \left[\varepsilon_{\text{CP}} \left(\frac{\eta_N}{\eta_N^{\text{eq}}} - 1 \right) - \frac{2}{3}\eta_{\Delta L} \right] - \frac{2}{3}\eta_{\Delta L} \left[\frac{\eta_N}{\eta_N^{\text{eq}}} \gamma_s + 2\gamma_t \right], \quad (4.3)$$

where $z \equiv m_N/T$ is a dimensionless parameter, $H_N \equiv H(z=1) \simeq 17m_N^2/M_{\text{Pl}}$ is the Hubble expansion rate at temperature $T = m_N$, $n_\gamma = 2T^3\zeta(3)/\pi^2$ is the number density of photons, and $\eta_N \equiv n_N/n_\gamma$ is the normalized number density of RHN (similarly $\eta_{\Delta L} = (n_L - n_{\bar{L}})/n_\gamma$ for the lepton asymmetry). The γ 's are the various thermalized interaction rates: γ_D for the RHN decay $N \rightarrow LH$, and $\gamma_s = \gamma_{Hs} + \gamma_{Vs}$ and $\gamma_t = \gamma_{Ht} + \gamma_{Vt}$ the standard $\Delta L = 1$ scattering processes as in Refs. [29, 83] with the subscripts s, t denoting respectively the s and t -channel exchange of the SM Higgs doublet H or the SM gauge

bosons $V = W_i, B$ (with $i = 1, 2, 3$) before EWSB. Here the integration over different momenta has already been performed, assuming implicitly kinetic equilibrium. The new scattering processes in our model in Fig. 4 correspond to the scattering rates γ_{NN} , and all the corresponding reduced cross sections $\hat{\sigma}(NN \rightarrow f\bar{f}, Z'\phi, \phi\phi, \mathcal{S}\mathcal{S}^\dagger)$ are collected in Appendix B. The prefactor of 2 in Eq. (4.2) accounts for the reduction of RHN by unit of two [34]. The thermal corrections to the SM particles are included in the calculation [83, 84]. If the γ_{NN} term is comparable or larger than other terms on the r.h.s. of Eq. (4.2), these extra processes in Fig. 4 could significantly dilute the RHN number density before the sphaleron decoupling temperature $T_c \simeq 131.7$ GeV [85], thus potentially making type-I seesaw freeze-out leptogenesis ineffective. Then we can set limits on the heavy particle masses and the couplings in the conformal $U(1)_{B-L}$ model.

To be concrete, we consider two distinct scenarios, i.e. without and with the DM particle \mathcal{S} involved in the lepton asymmetry generation in the RHN decay, with the first one corresponding to the limit of $m_{\mathcal{S}} \gg m_N$ and the second one $m_{\mathcal{S}} \lesssim m_N$. In both of the two cases, the dilution effect depends on the effective neutrino mass $\tilde{m} \equiv v^2(Y_D^\dagger Y_D)_{11}/m_N$ (or effectively on the Yukawa coupling Y_D) and the CP asymmetry ε_{CP} . Since in this paper we are mostly concerned with the role of the new particles in the lepton asymmetry generation in RHN decay $N \rightarrow LH$, we will not consider the flavor structure details in the neutrino sector but fix $\tilde{m} \simeq \sqrt{\Delta m_{\text{atm}}^2} \simeq 50$ meV, without any significant tuning or cancellation in the type-I seesaw formula for light neutrino masses [35]. A large CP-asymmetry ε_{CP} can then be generated by the resonant enhancement mechanism, and go up to order one if $\Delta m_N \sim \Gamma_N$, with Γ_N is the averaged RHN decay width [30, 86]. For the sake of concreteness, we adopt the value of $\varepsilon_{\text{CP}} = 10^{-2}$ throughout this paper.

In the case without DM, the dilution effect depends also on the RHN mass m_N , the Z' mass $M_{Z'}$, the conformal scalar mass m_ϕ , the quartic coupling λ_ϕ , with the last three being functions of the gauge coupling g_{BL} and the $B-L$ scale v_{BL} in the conformal theory, as shown in Eqs. (2.8), (2.9) and (2.6). Therefore we choose the free parameters to be m_N , g_{BL} and v_{BL} in the conformal model, with the Yukawa coupling Y_ϕ determined by the RHN mass for fixed v_{BL} which enters some of the diagrams in Fig. 4. For the three benchmark values of $g_{BL} = 0.1, 0.3, 1$ in Table 2, the LHC dilepton limits on v_{BL} are shown as the horizontal dashed red, green and blue lines in the left panel of Fig. 5. As stated in Ref. [35], in the case without DM, if the RHN mass $m_N \lesssim m_\phi$ and $2m_N \lesssim m_\phi + M_{Z'}$, the dilution is dominated by the Z' mediated process $NN \rightarrow f\bar{f}$, benefiting from the (almost) massless fermions in the final states and the large number of degrees of freedom. One can see the clear resonance structure in the left panel of Fig. 5; this corresponds to the inverse decay process $NN \rightarrow Z'$ with the subsequent decay of the on-shell Z' boson into SM fermions, which enhance largely the dilution effect. For heavy enough RHNs with $m_N \gtrsim m_\phi$ and/or $2m_N \gtrsim m_\phi + M_{Z'}$, the processes $NN \rightarrow \phi\phi$ and/or $NN \rightarrow Z'\phi$ are also important, which however is suppressed by the small Yukawa coupling Y_ϕ when $m_N \ll v_{BL}$. In the left

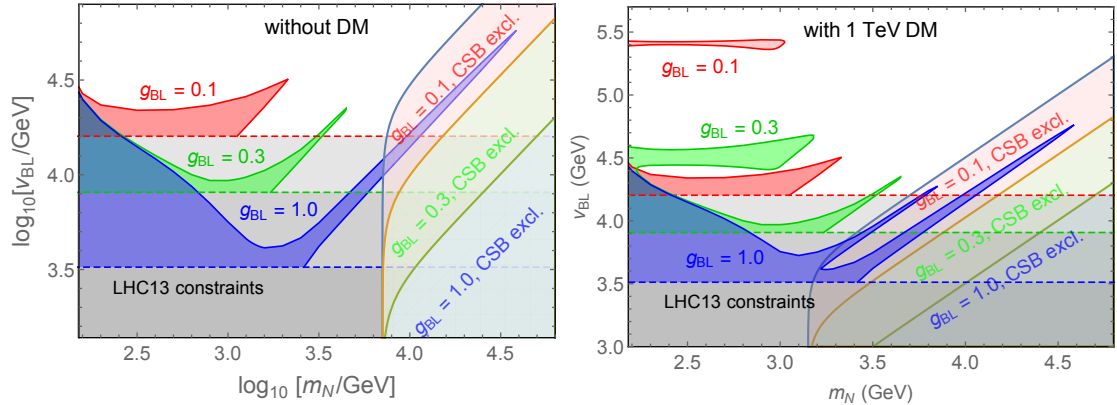


Figure 5. Parameter space for leptogenesis for the case without DM (left) and with a 1 TeV DM. The gray regions are excluded by the dilepton limits on the Z' mass (cf. Fig. 2 and Table 2), and the red, green and blue shaded regions are falsified by the processes shown in Fig. 4, with respectively $g_{BL} = 0.1, 0.3$ and 1. The lighter shaded regions are excluded by the condition $m_\phi^2 > 0$ in Eq. (2.9). For the case with DM, we have taken the DM mass to be 1 TeV.

panel of Fig. 5, all the red, green and blue shaded regions are falsified by the extra diluting processes.

When the DM mass $m_S \lesssim M_N$, the process $NN \rightarrow \mathcal{S}\mathcal{S}^\dagger$ would contribute to the dilution of lepton asymmetry generation, which is mediated by the Z' and ϕ bosons, with the Feynman diagrams shown in (f) and (g) in Fig. 4. With the dashed curves in Fig. 2, the dilepton limits on the Z' mass and the v_{BL} scale are slightly lower than the case without DM, as shown in Table 2. The Z' mediated process $NN \rightarrow Z' \rightarrow \mathcal{S}\mathcal{S}^\dagger$, however, can not compete the processes $NN \rightarrow ff$, as a result of the large degrees of freedom in the SM, unless the $B - L$ charge n_x of DM is very large. On the other hand, the cross section $\sigma(NN \rightarrow \phi \rightarrow \mathcal{S}\mathcal{S}^\dagger)$ in the scalar portal is proportional to the trilinear scalar coupling $(\lambda_{\phi S} v_{BL})^2$, which might enhance significantly the cross section when the v_{BL} scale is large. Compared to the case without DM, the new scalar portal opens the possibility of new resonance, due to the resonance relation $2E_N \simeq m_\phi$ (with E_N the RHN energy) before the RHN decays. This corresponds to the extra peak structures in the right panel of Fig. 5, where we have fixed the DM mass $m_S = 1$ TeV for the sake of concreteness. As in the left panel, all the red, green and blue shaded regions are falsified by the diluting processes which reduce the RHN number by two units.

In short, all the gray and red, green and blue shaded regions in both of the two panels of Fig. 5 are falsified by the Feynman diagrams in Fig. 4; to have a viable leptogenesis framework to generate the baryon asymmetry in the early Universe, one has to choose parameters in the unshaded regions in Fig. 5. Roughly speaking, when the gauge coupling g_{BL} (and the quartic coupling $\lambda_{\phi S}$) gets larger, the (reduced) cross sections for the dilution processes becomes larger, and the allowed parameter space shrinks significantly, depending

on the RHN mass M_N . The bounds from the correct spontaneous symmetry breaking condition imposed by $m_\phi^2 > 0$ (see Eq. (2.9)) are also presented in both the two panels of Fig. 5, which exclude the large m_N regions and are largely complementary to the limits from leptogenesis.

5 WIMP DM in the conformal $U(1)_{B-L}$ model

In this section, we investigate the DM phenomenology in the conformal $U(1)_{B-L}$ model, including the relic density of DM, direct detection and collider prospects.

5.1 Relic density and direct detection

For the GW favored benchmark scenarios, as explored in Fig. 3, DM annihilation at freezing-out is dominated by the process $\mathcal{S}\mathcal{S}^\dagger \rightarrow Z'Z'$, and a larger $U(1)_{B-L}$ charge n_x leads to a smaller annihilation cross section, which will yield a lower value for the relic abundance of DM. The corresponding Boltzmann equation is then given by

$$\frac{dY_S}{dx} = -\frac{1}{x^2} \frac{s(m_S)}{H(m_S)} \left[\langle \sigma v \rangle_{\mathcal{S}\mathcal{S}^\dagger \rightarrow Z'Z'} \left(Y_S^2 - \frac{(Y_S^{\text{eq}})^2}{(Y_{Z'}^{\text{eq}})^2} Y_{Z'}^2 \right) \right], \quad (5.1)$$

with $x \equiv m_S/T$ and the entropy density s and Hubble parameter H at the DM mass m_S are respectively

$$s(m_S) = \frac{2\pi^2}{45} g_* m_S^3, \quad H(m_S) = \frac{\pi}{\sqrt{90}} \frac{\sqrt{g_*}}{M_{\text{pl}}^r} m_S^2,$$

where $M_{\text{pl}}^r = 2.44 \times 10^{18}$ GeV is the reduced Planck mass. $Y_{S,Z'}^{\text{eq}}$ are respectively the equilibrium number densities of \mathcal{S} and Z' per comoving volume. $\langle \sigma v \rangle$ in Eq. (5.1) is the thermal averaged cross section and its expression is given in Appendix C. After freezing-out, the total relic abundance of DM at the present epoch is obtained through the following equation [87]

$$\Omega_{DM} h^2 = 2.755 \times 10^8 \left(\frac{m_S}{\text{GeV}} \right) Y_S(T_0), \quad (5.2)$$

with $Y_S(T_0)$ obtained from numerical solutions of the coupled Boltzmann equations given in Eq. (5.1).

Regarding the direct detection of DM, the spin-independent (SI) process is dominated by the Z' mediated scattering of DM off the nucleon \mathcal{N} , with the cross section

$$\sigma^{\text{SI}} \sim \frac{g_{BL}^4 n_x^2 m_{\mathcal{N}}^2}{M_{Z'}^4}. \quad (5.3)$$

A large n_x here can result in a large cross section, which is excluded by LUX [42], PandaX-II [43, 44] and Xenon1T [45]. Therefore, we do not expect the DM scalar \mathcal{S} under study will saturate all the observed DM relic abundance.

5.2 Collider signatures

The DM scalar \mathcal{S} can be produced at high-energy colliders in the scalar portal or the gauge portal. In the scalar portal, \mathcal{S} and \mathcal{S}^\dagger can be pair produced through both the SM Higgs h and the scalar ϕ , assisted by the $h - \phi$ mixing which is induced by the λ_P term in the potential (2.1). In particular, the most important production channel is from the gluon-fusion production of SM Higgs h or ϕ , associated with a gluon jet emitted from the initial partons, i.e.

$$gg \rightarrow g(h/\phi) \rightarrow g\mathcal{S}\mathcal{S}^\dagger. \quad (5.4)$$

The DM particles \mathcal{S} and \mathcal{S}^\dagger leaves the detectors without leaving any signal or track, and we have a high-energy jet with large missing transverse energy at colliders. However, the production cross section is suppressed by the effective loop-level couplings of h and ϕ to gluons, and the LHC monojet data can not set limits on the DM sector in the $U(1)_{B-L}$ model [38–41]. In the gauge portal, the most efficient way to produce DM \mathcal{S} is from the on-shell Z' decay in the process

$$q\bar{q} \rightarrow gZ', \quad Z' \rightarrow \mathcal{S}\mathcal{S}^\dagger. \quad (5.5)$$

In light of the current stringent limits on the Z' boson mass [49, 50], as shown in Fig. 2, the monojet searches at LHC are too weak to set any limit on the DM sector [38–41].

6 Conclusion

In this paper we introduce a hidden scalar \mathcal{S} to the $U(1)_{B-L}$ extension of the SM with classical conformal symmetry, which affects the dynamical EWSB by dimensional transmutation through the Coleman-Weinberg mechanism. The correct spontaneous symmetry breaking of the $U(1)_{B-L}$ symmetry restricts the scales of the hidden scalar and the RHNs. For smaller gauge coupling g_{BL} , a lower hidden scalar mass is crucial to realize a strong first order phase transition, and produce a GW signal to be probed by LISA. The possibility to realize the resonant leptogenesis mechanism is found to be disturbed by the hidden scalar depending on the mass hierarchy between it and the RHN. For the benchmark scenarios that can produce the LISA detectable GW signal and explain the baryon asymmetry of the Universe via resonant leptogenesis, we do not expect the dark matter relic abundance to be fully saturated by the hidden scalar introduced here.

Acknowledgments

The work of L.B. is supported by the National Natural Science Foundation of China under grant No.11605016 and No.11647307. W.C. is supported by the China Postdoctoral Science Foundation under Grant No.2019TQ0329. H.G. is partially supported by the U.S.

Department of Energy grant DE-SC0009956. Y.Z. is supported by the US Department of Energy under Grant No. DE-SC0017987, and would like to thank the Center for High Energy Physics, Peking University, the Institute of Theoretical Physics, Chinese Academy of Sciences, the Tsung-Dao Lee Institute, and the Institute of High Energy Physics, Chinese Academy of Sciences for generous hospitality where the paper was partially done.

A Renormalization group equations

Following Ref. [88], the RGEs for the scalar quartic couplings in the conformal $U(1)_{B-L}$ model read

$$\frac{d\lambda_x}{d\log\mu} = \beta_{\lambda_x}, \quad (\text{A.1})$$

with

$$16\pi^2\beta_{\lambda_H} = -6y_t^4 + 24\lambda_H^2 + \lambda_P^2 + \lambda_{HS}^2 + \lambda_H \left(12y_t^2 - \frac{9}{5}g_1^2 - 9g_2^2 \right) + \frac{27}{200}g_1^4 + \frac{9}{20}g_2^2g_1^2 + \frac{9}{8}g_2^4, \quad (\text{A.2})$$

$$16\pi^2\beta_{\lambda_\phi} = 20\lambda_\phi^2 + 2\lambda_P^2 + \lambda_{\phi S}^2 - 48\lambda_\phi g_{BL}^2 + 96g_{BL}^4 - \text{Tr}[Y_\phi Y_\phi^\top Y_\phi Y_\phi^\top] + 8\lambda_\phi \text{Tr}[Y_\phi Y_\phi^\top], \quad (\text{A.3})$$

$$16\pi^2\beta_{\lambda_P} = \lambda_P \left(6y_t^2 + 12\lambda_H + 8\lambda_\phi - 4\lambda_P - 24g_{BL}^2 - \frac{9}{10}g_1^2 - \frac{9}{2}g_2^2 + 4\text{Tr}[Y_\phi Y_\phi^\top] \right) - 2\lambda_{HS}\lambda_{\phi S}, \quad (\text{A.4})$$

$$16\pi^2\beta_{\lambda_S} = 20\lambda_S^2 + \lambda_{\phi S}^2 + 2\lambda_{HS}^2 + 6(n_x g_{BL})^4 - 12\lambda_s(n_x g_{BL})^2, \quad (\text{A.5})$$

$$16\pi^2\beta_{\lambda_{HS}} = \lambda_{HS} \left(6y_t^2 + 12\lambda_H + 6\lambda_S + 4\lambda_{HS} - \frac{9}{10}g_1^2 - \frac{9}{2}g_2^2 \right) - 2\lambda_P\lambda_{\phi S}, \quad (\text{A.6})$$

$$16\pi^2\beta_{\lambda_{\phi S}} = \lambda_{\phi S} (12\lambda_\phi + 6\lambda_S + 4\lambda_{\phi S} - 18g_{BL}^2) - 4\lambda_P\lambda_{HS}, \quad (\text{A.7})$$

where $g_1^2 = 5g_Y^2/3$ with $g_{2,Y}$ the gauge coupling for the SM gauge groups $SU(2)_L$ and $U(1)_Y$, y_t is the SM top Yukawa coupling. For simplicity we have neglected all other Yukawa couplings in the SM as well as the couplings Y_D which are much smaller. For the top quark Yukawa coupling y_t and the Y_ϕ coupling for the three RHNs, the RGEs are respectively

$$16\pi^2\beta_{y_t} = y_t \left(\frac{9}{2}y_t^2 - \frac{17}{20}g_1^2 - \frac{9}{4}g_2^2 - 8g_3^2 - \frac{2}{3}g_{BL}^2 \right), \quad (\text{A.8})$$

$$16\pi^2\beta_{Y_\phi} = Y_\phi \left(4Y_\phi Y_\phi^\top + \text{Tr}[Y_\phi Y_\phi^\top] - 6g_{BL}^2 \right), \quad (\text{A.9})$$

and the RGEs for the gauge couplings are given by

$$\begin{aligned} 16\pi^2\beta_{g_{BL}} &= 12g_{BL}^3, & 16\pi^2\beta_{g_3} &= -7g_3^3, \\ 16\pi^2\beta_{g_2} &= -\frac{19}{6}g_2^3, & 16\pi^2\beta_{g_1} &= \frac{41}{10}g_1^3, \end{aligned} \quad (\text{A.10})$$

where g_3 the gauge coupling for the SM gauge group $SU(3)_C$.

B Reduced cross sections for leptogenesis

In this appendix, we list the explicit analytic formulas for the reduced cross sections for various $2 \leftrightarrow 2$ scatterings involving the RHNs used in our leptogenesis calculations in Sec. 4. All the relevant Feynman diagrams can be found in Fig. 4. For the fermionic channels,

$$\hat{\sigma}(NN \rightarrow f\bar{f}) = \frac{S_f N_C^f (B_f - L_f)^2 g_{BL}^4 \sqrt{x}(x-4)^{3/2}}{96\pi |x-w|^2}, \quad (\text{B.1})$$

with $x = s/m_N^2$, $w = M_{Z'}^2/m_N^2$, and the symmetry factor $S_f = 1$ for the charged fermions and $1/4$ for neutrinos. For the bosonic channels,

$$\hat{\sigma}(NN \rightarrow \phi\phi) = \frac{Y_\phi^4}{32\pi} \left(\mathcal{A}_{SS}^{(1)} + \mathcal{A}_{SS}^{(2)} + \mathcal{A}_{SS}^{(3)} \right), \quad (\text{B.2})$$

$$\hat{\sigma}(NN \rightarrow Z'\phi) = \frac{g_{BL}^2}{64\pi w^2} \left(\mathcal{A}_{VS}^{(1)} + \mathcal{A}_{VS}^{(2)} + \mathcal{A}_{VS}^{(3)} \right), \quad (\text{B.3})$$

with the \mathcal{A}_{SS} and \mathcal{A}_{VS} terms

$$\mathcal{A}_{SS}^{(1)} \equiv \frac{121\beta_1(x-4)r^2}{|x-r|^2}, \quad (\text{B.4})$$

$$\mathcal{A}_{SS}^{(2)} \equiv -\frac{22r}{x(x-r)} \left[2\beta_1 x - (x+2(r-4)) \log \left(\frac{(1-\beta_1)x-2r}{(1+\beta_1)x-2r} \right) \right], \quad (\text{B.5})$$

$$\begin{aligned} \mathcal{A}_{SS}^{(3)} \equiv & -\beta_1 \left(1 + \frac{2(r-4)^2}{(x-2r)^2 - \beta_1^2 x^2} \right) - \frac{1}{2x(x-2r)} \left(x^2 - 4(r-4)x + 2(r-4)(3r+4) \right) \\ & \times \log \left(\frac{(1-\beta_1)x-2r}{(1+\beta_1)x-2r} \right), \end{aligned} \quad (\text{B.6})$$

$$\begin{aligned} \mathcal{A}_{VS}^{(1)} = & \frac{\beta_3 g_{BL}^2}{(x-w)^2} \left[4x^3 + ((w-16)w-8r)x^2 \right. \\ & + 2(2r^2 - r(w-4)w + w^2(3w+10))x \\ & \left. + w(r^2(w-8) - 2r(w-8)w + (w-40)w^2) - \frac{1}{3}\beta_3^2 w^2 x^2 \right], \end{aligned} \quad (\text{B.7})$$

$$\begin{aligned} \mathcal{A}_{VS}^{(2)} = & -\frac{4\sqrt{2}g_{BL}Y_\phi\sqrt{w}}{x(x-w)} \left[\beta_3 x (x^2 - (r+w)x + 4w^2) \right. \\ & + 2 \left(x^2 + (r(w-2) - w(w+2))x + r^2 - rw(w+2) - (w-9)w^2 \right) \\ & \left. \times \log \left(\frac{(1-\beta_3)x - (r+w)}{(1+\beta_3)x - (r+w)} \right) \right], \end{aligned} \quad (\text{B.8})$$

$$\begin{aligned} \mathcal{A}_{VS}^{(3)} = & 2Y_\phi^2 w \left[\beta_3 \left(x - 2w - \frac{4(4-r)(4-w)w}{(x-r-w)^2 - \beta_3^2 x^2} \right) \right. \\ & - \frac{1}{x(x-r-w)} \left((w-2)x^2 - 2(2r(w-1) + (w-10)w)x \right. \\ & \left. \left. + r^2(w-2) + 4rw(w-1) + w((w-10)w-32) \right) \right. \\ & \left. \times \log \left(\frac{(1-\beta_3)x - (r+w)}{(1+\beta_3)x - (r+w)} \right) \right], \end{aligned} \quad (\text{B.9})$$

where $r = m_\phi^2/m_N^2$ and

$$\beta_1 = \sqrt{(1-4x^{-1})(1-4rx^{-1})}, \quad (\text{B.10})$$

$$\beta_3 = \frac{1}{x} \sqrt{(1-4x^{-1})(x^2+r^2+w^2-2xr-2xw-2rw)}. \quad (\text{B.11})$$

At the Z' resonance, i.e. $M_{Z'} \simeq 2m_N$, the propagator $1/|x-w|$ should be modified accordingly to include the Z' width. For the DM channel,

$$\begin{aligned} \hat{\sigma}(NN \rightarrow \mathcal{S}\mathcal{S}^\dagger) &= \frac{\beta_2 n_x^2 g_{BL}^4}{768\pi|x-w|^2} [(3-\beta_2^2)x^2 + 48y - 12x(1+y)] \\ &\quad + \frac{\beta_2 \lambda_\phi^2 (x-4)}{16\pi|x-r|^2}, \end{aligned} \quad (\text{B.12})$$

with $y = m_S^2/m_N^2$, and

$$\beta_2 = \sqrt{(1-4x^{-1})(1-4yx^{-1})}. \quad (\text{B.13})$$

C DM annihilation cross section

Once the kinematical threshold $m_S > m_{Z'}$ is open, the dominant contribution to the DM pairs annihilations channel is $S(p_1)S^\dagger(p_2) \rightarrow Z'(p_3)Z'(p_4)$, with $p_{1,2,3,4}$ the corresponding momenta of incoming and outgoing particles. The squared amplitude is calculated using CalcHEP [89] with model files prepared by FeynRules [90],

$$\begin{aligned} |\mathcal{M}(SS^\dagger \rightarrow Z'Z')|^2 &= \frac{1}{8} \left[4\lambda_{\phi S}^2 + 64g_{DM}^4 + \frac{\lambda_{\phi S}^2 M_{Z'}^2 (16g_{BL}^4 (3M_{Z'}^2 - s) + \lambda_2^2 M_{Z'}^2)}{g_{BL}^4 (M_{H_2}^2 - s)^2} + \frac{4\lambda_2 \lambda_{\phi S}^2 M_{Z'}^2}{g_{BL}^2 (s - M_{H_2}^2)} \right. \\ &\quad + \frac{4g_{DM}^4 (6m_S^2 + 3M_{Z'}^2 - 2(s+t))^2}{(-m_S^2 - 2M_{Z'}^2 + s+t)^2} + \frac{4g_{DM}^4 (-2m_S^2 + M_{Z'}^2 - 2t)^2}{(m_S^2 - t)^2} \\ &\quad - \frac{8g_{DM}^4 (-4m_S^2 + M_{Z'}^2 + s)^2}{(m_S^2 - t)(m_S^2 + 2M_{Z'}^2 - s - t)} + \frac{(-4m_S^2 + 2M_{Z'}^2 + s - 4t)}{(M_{H_2}^2 - s)(m_S^2 - t)} \\ &\quad \times 8g_{DM}^2 \lambda_{\phi S} M_{Z'}^2 - \frac{8g_{DM}^2 \lambda_{\phi S} M_{Z'}^2 (12m_S^2 + 6M_{Z'}^2 - 5s - 4t)}{(M_{H_2}^2 - s)(-m_S^2 - 2M_{Z'}^2 + s + t)} \\ &\quad + \frac{1}{(M_{H_2}^2 - s)(m_S^2 - t)(-m_S^2 - 2M_{Z'}^2 + s + t)} \\ &\quad \times \left(8g_{DM}^2 (g_{DM}^2 (M_{H_2}^2 - s)(8m_S^4 - 16m_S^2 t + 4M_{Z'}^4 - 16M_{Z'}^2 t \right. \\ &\quad \left. - s^2 + 8st + 8t^2) + 16\lambda_{\phi S} M_{Z'}^2 (m_S^2 + 2M_{Z'}^2 - s - t)(m_S^2 - t) \right) \left. \right], \quad (\text{C.1}) \end{aligned}$$

with

$$s = (p_1 + p_2)^2 = (p_3 + p_4)^2, \quad (\text{C.2})$$

$$t = (p_1 - p_3)^2 = (p_4 - p_2)^2. \quad (\text{C.3})$$

Here, the $m_{H_2} \approx m_\phi$ for small mixing between the SM Higgs h and the $B - L$ Higgs ϕ . With the squared amplitude at hand, the cross section is given by

$$\sigma(SS^\dagger \rightarrow Z'Z') = \frac{1}{64\pi^2} \frac{\sqrt{1 - 4M_{Z'}^2/s}}{1 - 4m_S^2/s} \int d\Omega |\mathcal{M}(SS^\dagger \rightarrow Z'Z')|^2. \quad (\text{C.4})$$

The thermal averaged annihilation cross section $\langle\sigma v\rangle$ are obtained in terms of annihilation cross section and the second kind modified Bessel function [91]

$$\langle\sigma v\rangle = \frac{1}{8m_S^4 T K_2^2\left(\frac{m_S}{T}\right)} \int_{4m_S^2}^{\infty} \sigma(s - 4m_S^2) \sqrt{s} K_1\left(\frac{\sqrt{s}}{T}\right) ds. \quad (\text{C.5})$$

References

- [1] S. R. Coleman and E. J. Weinberg, “Radiative Corrections as the Origin of Spontaneous Symmetry Breaking,” *Phys. Rev.* **D7** (1973) 1888–1910.
- [2] C. Englert, J. Jaeckel, V. V. Khoze, and M. Spannowsky, “Emergence of the Electroweak Scale through the Higgs Portal,” *JHEP* **04** (2013) 060, [arXiv:1301.4224 \[hep-ph\]](#).
- [3] A. Farzinnia, H.-J. He, and J. Ren, “Natural Electroweak Symmetry Breaking from Scale Invariant Higgs Mechanism,” *Phys. Lett.* **B727** (2013) 141–150, [arXiv:1308.0295 \[hep-ph\]](#).
- [4] V. V. Khoze, “Inflation and Dark Matter in the Higgs Portal of Classically Scale Invariant Standard Model,” *JHEP* **11** (2013) 215, [arXiv:1308.6338 \[hep-ph\]](#).
- [5] S. Iso, N. Okada, and Y. Orikasa, “Classically conformal $B - L$ extended Standard Model,” *Phys. Lett.* **B676** (2009) 81–87, [arXiv:0902.4050 \[hep-ph\]](#).
- [6] **LISA** Collaboration, H. Audley *et al.*, “Laser Interferometer Space Antenna,” [arXiv:1702.00786 \[astro-ph.IM\]](#).
- [7] T. Robson, N. J. Cornish, and C. Liug, “The construction and use of LISA sensitivity curves,” *Class. Quant. Grav.* **36** no. 10, (2019) 105011, [arXiv:1803.01944 \[astro-ph.HE\]](#).
- [8] X. Gong *et al.*, “Descope of the ALIA mission,” *J. Phys. Conf. Ser.* **610** no. 1, (2015) 012011, [arXiv:1410.7296 \[gr-qc\]](#).
- [9] **TianQin** Collaboration, J. Luo *et al.*, “TianQin: a space-borne gravitational wave detector,” *Class. Quant. Grav.* **33** no. 3, (2016) 035010, [arXiv:1512.02076 \[astro-ph.IM\]](#).
- [10] V. Corbin and N. J. Cornish, “Detecting the cosmic gravitational wave background with the big bang observer,” *Class. Quant. Grav.* **23** (2006) 2435–2446, [arXiv:gr-qc/0512039 \[gr-qc\]](#).
- [11] **DECIGO Working group** Collaboration, M. Musha, “Space gravitational wave detector DECIGO/pre-DECIGO,” *Proc. SPIE Int. Soc. Opt. Eng.* **10562** (2017) 105623T.
- [12] H. Kudoh, A. Taruya, T. Hiramatsu, and Y. Himemoto, “Detecting a gravitational-wave background with next-generation space interferometers,” *Phys. Rev.* **D73** (2006) 064006, [arXiv:gr-qc/0511145 \[gr-qc\]](#).

- [13] J. Ellis, M. Lewicki, J. M. No, and V. Vaskonen, “Gravitational wave energy budget in strongly supercooled phase transitions,” *JCAP* **1906** no. 06, (2019) 024, [arXiv:1903.09642 \[hep-ph\]](#).
- [14] J. Ellis, M. Lewicki, and J. M. No, “On the Maximal Strength of a First-Order Electroweak Phase Transition and its Gravitational Wave Signal,” [arXiv:1809.08242 \[hep-ph\]](#). [JCAP1904,003(2019)].
- [15] R. Jinno and M. Takimoto, “Probing a classically conformal B-L model with gravitational waves,” *Phys. Rev.* **D95** no. 1, (2017) 015020, [arXiv:1604.05035 \[hep-ph\]](#).
- [16] S. Iso, P. D. Serpico, and K. Shimada, “QCD-Electroweak First-Order Phase Transition in a Supercooled Universe,” *Phys. Rev. Lett.* **119** no. 14, (2017) 141301, [arXiv:1704.04955 \[hep-ph\]](#).
- [17] W. Chao, H.-K. Guo, and J. Shu, “Gravitational Wave Signals of Electroweak Phase Transition Triggered by Dark Matter,” *JCAP* **1709** no. 09, (2017) 009, [arXiv:1702.02698 \[hep-ph\]](#).
- [18] W. Chao, W.-F. Cui, H.-K. Guo, and J. Shu, “Gravitational Wave Imprint of New Symmetry Breaking,” [arXiv:1707.09759 \[hep-ph\]](#).
- [19] P. Minkowski, “ $\mu \rightarrow e\gamma$ at a Rate of One Out of 10^9 Muon Decays?,” *Phys. Lett.* **67B** (1977) 421–428.
- [20] R. N. Mohapatra and G. Senjanovic, “Neutrino Mass and Spontaneous Parity Nonconservation,” *Phys. Rev. Lett.* **44** (1980) 912. [231(1979)].
- [21] T. Yanagida, “Horizontal gauge symmetry and masses of neutrinos,” *Conf. Proc.* **C7902131** (1979) 95–99.
- [22] M. Gell-Mann, P. Ramond, and R. Slansky, “Complex Spinors and Unified Theories,” *Conf. Proc.* **C790927** (1979) 315–321, [arXiv:1306.4669 \[hep-th\]](#).
- [23] S. L. Glashow, “The Future of Elementary Particle Physics,” *NATO Sci. Ser. B* **61** (1980) 687.
- [24] M. Fukugita and T. Yanagida, *Phys. Lett. B* **174**, 45 (1986).
- [25] V. V. Khoze and G. Ro, “Leptogenesis and Neutrino Oscillations in the Classically Conformal Standard Model with the Higgs Portal,” *JHEP* **10** (2013) 075, [arXiv:1307.3764 \[hep-ph\]](#).
- [26] L. Covi, E. Roulet, and F. Vissani, “CP violating decays in leptogenesis scenarios,” *Phys. Lett.* **B384** (1996) 169–174, [arXiv:hep-ph/9605319 \[hep-ph\]](#).
- [27] M. Flanz, E. A. Paschos, U. Sarkar, and J. Weiss, “Baryogenesis through mixing of heavy Majorana neutrinos,” *Phys. Lett.* **B389** (1996) 693–699, [arXiv:hep-ph/9607310 \[hep-ph\]](#).
- [28] A. Pilaftsis, “CP violation and baryogenesis due to heavy Majorana neutrinos,” *Phys. Rev.* **D56** (1997) 5431–5451, [arXiv:hep-ph/9707235 \[hep-ph\]](#).
- [29] A. Pilaftsis and T. E. J. Underwood, “Resonant leptogenesis,” *Nucl. Phys.* **B692** (2004) 303–345, [arXiv:hep-ph/0309342 \[hep-ph\]](#).

- [30] S. Blanchet, Z. Chacko, S. S. Granor, and R. N. Mohapatra, “Probing Resonant Leptogenesis at the LHC,” *Phys. Rev.* **D82** (2010) 076008, [arXiv:0904.2174 \[hep-ph\]](#).
- [31] S. Blanchet, P. S. B. Dev, and R. N. Mohapatra, “Leptogenesis with TeV Scale Inverse Seesaw in SO(10),” *Phys. Rev.* **D82** (2010) 115025, [arXiv:1010.1471 \[hep-ph\]](#).
- [32] S. Iso, N. Okada, and Y. Orikasa, “Resonant Leptogenesis in the Minimal B-L Extended Standard Model at TeV,” *Phys. Rev.* **D83** (2011) 093011, [arXiv:1011.4769 \[hep-ph\]](#).
- [33] N. Okada, Y. Orikasa, and T. Yamada, “Minimal Flavor Violation in the Minimal $U(1)_{B-L}$ Model and Resonant Leptogenesis,” *Phys. Rev.* **D86** (2012) 076003, [arXiv:1207.1510 \[hep-ph\]](#).
- [34] J. Heeck and D. Teresi, “Leptogenesis and neutral gauge bosons,” *Phys. Rev.* **D94** no. 9, (2016) 095024, [arXiv:1609.03594 \[hep-ph\]](#).
- [35] P. S. B. Dev, R. N. Mohapatra, and Y. Zhang, “Leptogenesis constraints on $B - L$ breaking Higgs boson in TeV scale seesaw models,” *JHEP* **03** (2018) 122, [arXiv:1711.07634 \[hep-ph\]](#).
- [36] T. Hambye, A. Strumia, and D. Teresi, “Super-cool Dark Matter,” *JHEP* **08** (2018) 188, [arXiv:1805.01473 \[hep-ph\]](#).
- [37] W. Rodejohann and C. E. Yaguna, “Scalar dark matter in the B-L model,” *JCAP* **1512** no. 12, (2015) 032, [arXiv:1509.04036 \[hep-ph\]](#).
- [38] **CMS** Collaboration, V. Khachatryan *et al.*, “Search for dark matter, extra dimensions, and unparticles in monojet events in proton-proton collisions at $\sqrt{s} = 8$ TeV,” *Eur. Phys. J.* **C75** no. 5, (2015) 235, [arXiv:1408.3583 \[hep-ex\]](#).
- [39] **ATLAS** Collaboration, G. Aad *et al.*, “Search for new phenomena in final states with an energetic jet and large missing transverse momentum in pp collisions at $\sqrt{s} = 8$ TeV with the ATLAS detector,” *Eur. Phys. J.* **C75** no. 7, (2015) 299, [arXiv:1502.01518 \[hep-ex\]](#). [Erratum: *Eur. Phys. J.* **C75**, no. 9, 408 (2015)].
- [40] **ATLAS** Collaboration, M. Aaboud *et al.*, “Search for dark matter and other new phenomena in events with an energetic jet and large missing transverse momentum using the ATLAS detector,” *JHEP* **01** (2018) 126, [arXiv:1711.03301 \[hep-ex\]](#).
- [41] **CMS** Collaboration, A. M. Sirunyan *et al.*, “Search for new physics in final states with an energetic jet or a hadronically decaying W or Z boson and transverse momentum imbalance at $\sqrt{s} = 13$ TeV,” *Phys. Rev.* **D97** no. 9, (2018) 092005, [arXiv:1712.02345 \[hep-ex\]](#).
- [42] **LUX** Collaboration, D. S. Akerib *et al.*, “Results from a search for dark matter in the complete LUX exposure,” *Phys. Rev. Lett.* **118** no. 2, (2017) 021303, [arXiv:1608.07648 \[astro-ph.CO\]](#).
- [43] **PandaX-II** Collaboration, A. Tan *et al.*, “Dark Matter Results from First 98.7 Days of Data from the PandaX-II Experiment,” *Phys. Rev. Lett.* **117** no. 12, (2016) 121303, [arXiv:1607.07400 \[hep-ex\]](#).
- [44] **PandaX-II** Collaboration, X. Cui *et al.*, “Dark Matter Results From 54-Ton-Day Exposure

- of PandaX-II Experiment,” *Phys. Rev. Lett.* **119** no. 18, (2017) 181302, [arXiv:1708.06917 \[astro-ph.CO\]](#).
- [45] **XENON** Collaboration, E. Aprile *et al.*, “First Dark Matter Search Results from the XENON1T Experiment,” *Phys. Rev. Lett.* **119** no. 18, (2017) 181301, [arXiv:1705.06655 \[astro-ph.CO\]](#).
- [46] A. Biswas, S. Choubey and S. Khan, *JHEP* **1608**, 114 (2016) [[arXiv:1604.06566 \[hep-ph\]](#)].
- [47] S. Patra, F. S. Queiroz, and W. Rodejohann, “Stringent Dilepton Bounds on Left-Right Models using LHC data,” *Phys. Lett.* **B752** (2016) 186–190, [arXiv:1506.03456 \[hep-ph\]](#).
- [48] M. Lindner, F. S. Queiroz, and W. Rodejohann, “Dilepton bounds on left-Right symmetry at the LHC run II and neutrinoless double beta decay,” *Phys. Lett.* **B762** (2016) 190–195, [arXiv:1604.07419 \[hep-ph\]](#).
- [49] **ATLAS** Collaboration, T. A. collaboration, “Search for new high-mass resonances in the dilepton final state using proton-proton collisions at $\sqrt{s} = 13$ TeV with the ATLAS detector,”.
- [50] **CMS** Collaboration, C. Collaboration, “Search for a high-mass resonance decaying into a dilepton final state in 13 fb^{-1} of pp collisions at $\sqrt{s} = 13$ TeV,”.
- [51] P. S. Bhupal Dev, R. N. Mohapatra, and Y. Zhang, “Naturally stable right-handed neutrino dark matter,” *JHEP* **11** (2016) 077, [arXiv:1608.06266 \[hep-ph\]](#).
- [52] R. Diener, S. Godfrey, and T. A. W. Martin, “Unravelling an Extra Neutral Gauge Boson at the LHC using Third Generation Fermions,” *Phys. Rev.* **D83** (2011) 115008, [arXiv:1006.2845 \[hep-ph\]](#).
- [53] S. Godfrey and T. Martin, “Z’ Discovery Reach at Future Hadron Colliders: A Snowmass White Paper,” in *Proceedings, 2013 Community Summer Study on the Future of U.S. Particle Physics: Snowmass on the Mississippi (CSS2013): Minneapolis, MN, USA, July 29-August 6, 2013*. 2013. [arXiv:1309.1688 \[hep-ph\]](#). <http://www.slac.stanford.edu/econf/C1307292/docs/submittedArxivFiles/1309.1688.pdf>.
- [54] T. G. Rizzo, “Exploring new gauge bosons at a 100 TeV collider,” *Phys. Rev.* **D89** no. 9, (2014) 095022, [arXiv:1403.5465 \[hep-ph\]](#).
- [55] J. Bernon, L. Bian, and Y. Jiang, “A new insight into the phase transition in the early Universe with two Higgs doublets,” *JHEP* **05** (2018) 151, [arXiv:1712.08430 \[hep-ph\]](#).
- [56] I. Affleck, “Quantum Statistical Metastability,” *Phys. Rev. Lett.* **46** (1981) 388.
- [57] A. D. Linde, “Decay of the False Vacuum at Finite Temperature,” *Nucl. Phys.* **B216** (1983) 421. [Erratum: *Nucl. Phys.*B223,544(1983)].
- [58] A. D. Linde, “Fate of the False Vacuum at Finite Temperature: Theory and Applications,” *Phys. Lett.* **100B** (1981) 37–40.
- [59] C. Caprini *et al.*, “Science with the space-based interferometer eLISA. II: Gravitational waves from cosmological phase transitions,” *JCAP* **1604** no. 04, (2016) 001, [arXiv:1512.06239 \[astro-ph.CO\]](#).

- [60] R.-G. Cai, Z. Cao, Z.-K. Guo, S.-J. Wang, and T. Yang, “The Gravitational-Wave Physics,” *Natl. Sci. Rev.* **4** no. 5, (2017) 687–706, [arXiv:1703.00187 \[gr-qc\]](#).
- [61] D. J. Weir, “Gravitational waves from a first order electroweak phase transition: a brief review,” *Phil. Trans. Roy. Soc. Lond.* **A376** no. 2114, (2018) 20170126, [arXiv:1705.01783 \[hep-ph\]](#).
- [62] M. Hindmarsh, S. J. Huber, K. Rummukainen, and D. J. Weir, “Gravitational waves from the sound of a first order phase transition,” *Phys. Rev. Lett.* **112** (2014) 041301, [arXiv:1304.2433 \[hep-ph\]](#).
- [63] M. Hindmarsh, S. J. Huber, K. Rummukainen, and D. J. Weir, “Numerical simulations of acoustically generated gravitational waves at a first order phase transition,” *Phys. Rev.* **D92** no. 12, (2015) 123009, [arXiv:1504.03291 \[astro-ph.CO\]](#).
- [64] R. Jinno and M. Takimoto, “Gravitational waves from bubble dynamics: Beyond the Envelope,” *JCAP* **1901** (2019) 060, [arXiv:1707.03111 \[hep-ph\]](#).
- [65] R. Jinno, S. Lee, H. Seong, and M. Takimoto, “Gravitational waves from first-order phase transitions: Towards model separation by bubble nucleation rate,” *JCAP* **1711** (2017) 050, [arXiv:1708.01253 \[hep-ph\]](#).
- [66] R. Jinno and M. Takimoto, “Gravitational waves from bubble collisions: An analytic derivation,” *Phys. Rev.* **D95** no. 2, (2017) 024009, [arXiv:1605.01403 \[astro-ph.CO\]](#).
- [67] D. Cutting, M. Hindmarsh, and D. J. Weir, “Gravitational waves from vacuum first-order phase transitions: from the envelope to the lattice,” *Phys. Rev.* **D97** no. 12, (2018) 123513, [arXiv:1802.05712 \[astro-ph.CO\]](#).
- [68] A. Kosowsky, M. S. Turner, and R. Watkins, “Gravitational radiation from colliding vacuum bubbles,” *Phys. Rev.* **D45** (1992) 4514–4535.
- [69] A. Kosowsky, M. S. Turner, and R. Watkins, “Gravitational waves from first order cosmological phase transitions,” *Phys. Rev. Lett.* **69** (1992) 2026–2029.
- [70] A. Kosowsky and M. S. Turner, “Gravitational radiation from colliding vacuum bubbles: envelope approximation to many bubble collisions,” *Phys. Rev.* **D47** (1993) 4372–4391, [arXiv:astro-ph/9211004 \[astro-ph\]](#).
- [71] S. J. Huber and T. Konstandin, “Gravitational Wave Production by Collisions: More Bubbles,” *JCAP* **0809** (2008) 022, [arXiv:0806.1828 \[hep-ph\]](#).
- [72] C. Caprini, R. Durrer, and G. Servant, “The stochastic gravitational wave background from turbulence and magnetic fields generated by a first-order phase transition,” *JCAP* **0912** (2009) 024, [arXiv:0909.0622 \[astro-ph.CO\]](#).
- [73] P. Binetruy, A. Bohe, C. Caprini, and J.-F. Dufaux, “Cosmological Backgrounds of Gravitational Waves and eLISA/NGO: Phase Transitions, Cosmic Strings and Other Sources,” *JCAP* **1206** (2012) 027, [arXiv:1201.0983 \[gr-qc\]](#).
- [74] J. R. Espinosa, T. Konstandin, J. M. No, and G. Servant, “Energy Budget of Cosmological First-order Phase Transitions,” *JCAP* **1006** (2010) 028, [arXiv:1004.4187 \[hep-ph\]](#).

- [75] A. Alves, T. Ghosh, H.-K. Guo, K. Sinha, and D. Vagie, “Collider and Gravitational Wave Complementarity in Exploring the Singlet Extension of the Standard Model,” *JHEP* **04** (2019) 052, [arXiv:1812.09333 \[hep-ph\]](#).
- [76] A. Alves, T. Ghosh, H.-K. Guo, and K. Sinha, “Resonant Di-Higgs Production at Gravitational Wave Benchmarks: A Collider Study using Machine Learning,” *JHEP* **12** (2018) 070, [arXiv:1808.08974 \[hep-ph\]](#).
- [77] A. Kosowsky, A. Mack, and T. Kahniashvili, “Gravitational radiation from cosmological turbulence,” *Phys. Rev.* **D66** (2002) 024030, [arXiv:astro-ph/0111483 \[astro-ph\]](#).
- [78] G. Gogoberidze, T. Kahniashvili, and A. Kosowsky, “The Spectrum of Gravitational Radiation from Primordial Turbulence,” *Phys. Rev.* **D76** (2007) 083002, [arXiv:0705.1733 \[astro-ph\]](#).
- [79] P. Niksa, M. Schlexer, and G. Sigl, “Gravitational Waves produced by Compressible MHD Turbulence from Cosmological Phase Transitions,” *Class. Quant. Grav.* **35** no. 14, (2018) 144001, [arXiv:1803.02271 \[astro-ph.CO\]](#).
- [80] A. R. Pol, S. Mandal, A. Brandenburg, T. Kahniashvili, and A. Kosowsky, “Numerical Simulations of Gravitational Waves from Early-Universe Turbulence,” [arXiv:1903.08585 \[astro-ph.CO\]](#).
- [81] A. Brandenburg, T. Kahniashvili, S. Mandal, A. R. Pol, A. G. Tevzadze, and T. Vachaspati, “Evolution of hydromagnetic turbulence from the electroweak phase transition,” *Phys. Rev.* **D96** no. 12, (2017) 123528, [arXiv:1711.03804 \[astro-ph.CO\]](#).
- [82] S. Davidson and A. Ibarra, “A Lower bound on the right-handed neutrino mass from leptogenesis,” *Phys. Lett.* **B535** (2002) 25–32, [arXiv:hep-ph/0202239 \[hep-ph\]](#).
- [83] G. F. Giudice, A. Notari, M. Raidal, A. Riotto, and A. Strumia, “Towards a complete theory of thermal leptogenesis in the SM and MSSM,” *Nucl. Phys.* **B685** (2004) 89–149, [arXiv:hep-ph/0310123 \[hep-ph\]](#).
- [84] P. S. Bhupal Dev, P. Millington, A. Pilaftsis, and D. Teresi, “Flavour Covariant Transport Equations: an Application to Resonant Leptogenesis,” *Nucl. Phys.* **B886** (2014) 569–664, [arXiv:1404.1003 \[hep-ph\]](#).
- [85] M. D’Onofrio, K. Rummukainen, and A. Tranberg, “Sphaleron Rate in the Minimal Standard Model,” *Phys. Rev. Lett.* **113** no. 14, (2014) 141602, [arXiv:1404.3565 \[hep-ph\]](#).
- [86] B. Dev, M. Garny, J. Klaric, P. Millington, and D. Teresi, “Resonant enhancement in leptogenesis,” *Int. J. Mod. Phys.* **A33** (2018) 1842003, [arXiv:1711.02863 \[hep-ph\]](#).
- [87] J. Edsjo and P. Gondolo, “Neutralino relic density including coannihilations,” *Phys. Rev.* **D56** (1997) 1879–1894, [arXiv:hep-ph/9704361 \[hep-ph\]](#).
- [88] V. V. Khoze, C. McCabe and G. Ro, *JHEP* **1408**, 026 (2014) [[arXiv:1403.4953 \[hep-ph\]](#)].
- [89] A. Belyaev, N. D. Christensen and A. Pukhov, *Comput. Phys. Commun.* **184**, 1729 (2013) doi:10.1016/j.cpc.2013.01.014 [[arXiv:1207.6082 \[hep-ph\]](#)].
- [90] A. Alloul, N. D. Christensen, C. Degrande, C. Duhr and B. Fuks, *Comput. Phys. Commun.* **185**, 2250 (2014) doi:10.1016/j.cpc.2014.04.012 [[arXiv:1310.1921 \[hep-ph\]](#)].

- [91] P. Gondolo and G. Gelmini, “Cosmic abundances of stable particles: Improved analysis,”
Nucl. Phys. **B360** (1991) 145–179.